Chemical Science

Cite this: *Chem. Sci.*, 2012, **3**, 2530

www.rsc.org/chemicalscience

EDGE ARTICLE

New tetrathiafulvalene fused-naphthalene diimides for solution-processible and air-stable p-type and ambipolar organic semiconductors†

Luxi Tan, Yunlong Guo, Yang Yang, Guanxin Zhang,* Deqing Zhang,* Gui Yu, Wei Xu and Yunqi Liu

Received 10th March 2012, Accepted 22nd May 2012
DOI: 10.1039/c2sc20303k

New conjugated electron donor–acceptor molecules with tetrathiafulvalene (TTF) fused-naphthalene diimide frameworks (**1–6**) are synthesized and investigated. The NDI cores are flanked by TTF and 2-(1,3-dithiol-2-ylidene)malonitrile moieties within **1–3**, whereas compounds **4–6** contain two TTF moieties. Based on cyclic voltammetric and absorption spectral studies, the LUMO and HOMO energies of **1–3** are estimated to be *ca.* −4.3 eV and *ca.* −5.1 eV, and those of **4–6** are *ca.* −4.1 eV and *ca.* −5.0 eV, respectively. These values are consistent with theoretical calculations. Thin films of **1–6** are easily prepared with the spin-coating technique and the resulting OFETs are successfully fabricated with conventional procedures. The OFETs results reveal that compounds **1–3** behave as ambipolar semiconductors and **4–6** as p-type semiconductors. Among **1–3**, compound **3** exhibits relatively high hole and electron mobilities in air, reaching 0.03 and 0.003 $cm^2\ V^{-1}\ s^{-1}$, respectively, after annealing at 160 °C. The OFET based on a thin film of **5** shows the best performance with $\mu_h = 0.31\ cm^2\ V^{-1}\ s^{-1}$, $I_{on/off} = 10^4$ among compounds **4–6** after annealing at 160 °C. The thin films of **1–6** are investigated with XRD and AFM, and the data can well interpret the variation of carrier mobilities of **1–6** after annealing. Moreover, the influences of alkyl chains in **1–6** on the intermolecular arrangements and carrier mobilities are also discussed.

Introduction

Organic semiconductors and the resulting organic field-effect transistors (OFETs) have drawn tremendous attentions in recent years because of their promising applications in a number of areas.[1–10] Both p- and n-type as well as ambipolar organic semiconductors have been reported in recent years. A number of organic p-type semiconductors of high hole-mobilities have been developed.[11–15] For instance, Takimiya and co-workers described a series of thiophene-containing conjugated molecules for p-type semiconductors which exhibit high hole-mobilities and good air stabilities.[16] In comparison, air-stable n-type organic semiconductors are still limited. This is mainly because of the fact that the respective anions of organic conjugated molecules are sensitive to oxygen and water.[17] The known organic n-type semiconductors are based on conjugated molecules with appropriate electron-withdrawing groups such as such as perylene diimides and naphthalene diimides.[18–21] Air-stable ambipolar organic semiconductors which are highly desired for molecular circuits have been intensively pursued in recent years.[22] Several diketopyrrolopyrrole (DPP) containing polymers were reported to be ambipolar semiconductors with hole and electron mobilities up to 0.3 $cm^2\ V^{-1}\ s^{-1}$ in inert atmosphere.[23–25] However, organic ambipolar semiconductors with high carrier mobilities in air are still quite limited. Sariciftci and co-workers reported indigo based ambipolar semiconductors with hole and electron mobilities up to 0.01 and 0.0045 $cm^2\ V^{-1}\ s^{-1}$ in air.[26]

Both experimental and theoretical efforts were made to correlate the chemical structures of conjugated molecules with the properties of organic semiconductors.[27,28] Nevertheless, it is still challenging to design conjugated molecules rationally for organic semiconductors with high mobilities. In this context, the conjugated electron donor–acceptor (D–A) frameworks deserve attention for designing new organic semiconductors based on the following considerations: (1) it is possible to tune the HOMO and LUMO energies deliberately by choosing appropriate electron donors and acceptors as well as the linkers that connect the electron donors and acceptors covalently. Such HOMO/LUMO energy modulation may enable the easy injection of electrons or holes from electrodes, thus leading to OFETs of high performance; (2) the intermolecular interaction among the D and A units may induce the neighboring molecules to arrange in an orderly manner, and such an intermolecular ordered arrangement is beneficial for enhancing the mobilities of organic semiconductors;[29] (3) it is expected that these conjugated D–A molecules may become ambipolar semiconductors when their

Beijing National Laboratory for Molecular Sciences, CAS Key Laboratories of Organic Solids, Institute of Chemistry, Chinese Academy of Sciences, Beijing 100190, China. E-mail: dqzhang@iccas.ac.cn

† Electronic supplementary information (ESI) available: General information for synthesis and characterization, UV-Vis absorption, TGA analysis, XRD patterns and AFM images, theoretical calculations data, ^1H NMR and ^{13}C NMR for compounds **1–6**. See DOI: 10.1039/c2sc20303k

HOMO/LUMO energies are appropriately balanced; (4) in principle, it is possible to change p-type semiconductors into n-type ones by linking strong electron acceptors to the conjugated molecular framework, and similarly transform n-type semiconductors into p-type ones by linking strong electron donors to the conjugated molecular framework.

1,4,5,8-Naphthalene diimide (NDI) and its derivatives have been intensively investigated for n-type semiconductors. It is common to design new n-type semiconductors that are stable under OFET device working conditions in air by incorporating electron-withdrawing groups into the NDI core to reduce the LUMO energy.[30] For instance, Gao *et al.* have recently reported core-expanded NDI derivatives containing 2-(1,3-dithiol-2-ylidene)malonitrile groups (electron-withdrawing) and the resulting OFETs exhibit electron mobilities up to 1.2 cm^2 V^{-1} s^{-1} in air.[31] However, NDI derivatives with electron donating groups are less explored. Some of us have just recently described NDI with 1,3-dithole-2-thione (-one) groups, but they still behave as n-type semiconductors.[32] In fact, NDI based p-type and ambipolar materials are seldom reported.[33,34]

In this paper we report two series of core-expanded NDI derivatives **1–3** and **4–6** (Scheme 1) with electron donating tetrathiafulvalene (TTF) moieties. Note that TTF and its derivatives have played important roles in the development of organic conducting materials for nearly four decades.[35–40] In recent years, TTF and its derivatives have been recognized as p-type semiconductors.[41] The incorporation of TTF units into the NDI core is based on the following considerations: (1) the introduction of TTF moieties might raise the HOMO levels and may eventually tune the core expanded NDI into ambipolar and p-type materials; (2) fusion of sulfur-rich TTF heterocycles with the NDI core would increase the intermolecular interactions which may be beneficial for improving the carrier mobilities of resulting semiconductors; (3) the presence of alkyl side-chains of different lengths in compounds **1–6** would not only improve their solubilities in organic solvents, but also affect the intermolecular arrangements, which will in turn have an effect on the carrier mobilities of the resulting semiconductors. In addition, 2-(1,3-dithiol-2-ylidene)malonitrile groups (electron-withdrawing moieties) are introduced into compounds **1–3** to finely tune the HOMO/LUMO energies.

The results reveal that compounds **1**, **2** and **3** exhibit ambipolar semiconducting properties and OFETs based on **3** exhibit hole and electron mobilities up to 0.03 and 0.003 cm^2 V^{-1} s^{-1} in air, respectively, which are among the highest mobilities for solution-processed ambipolar OFETs with small conjugated molecules in air.[26] By contrast, compounds **4**, **5** and **6** all behave as p-type semiconductors with hole mobilities up to 0.31 cm^2 V^{-1} s^{-1}.

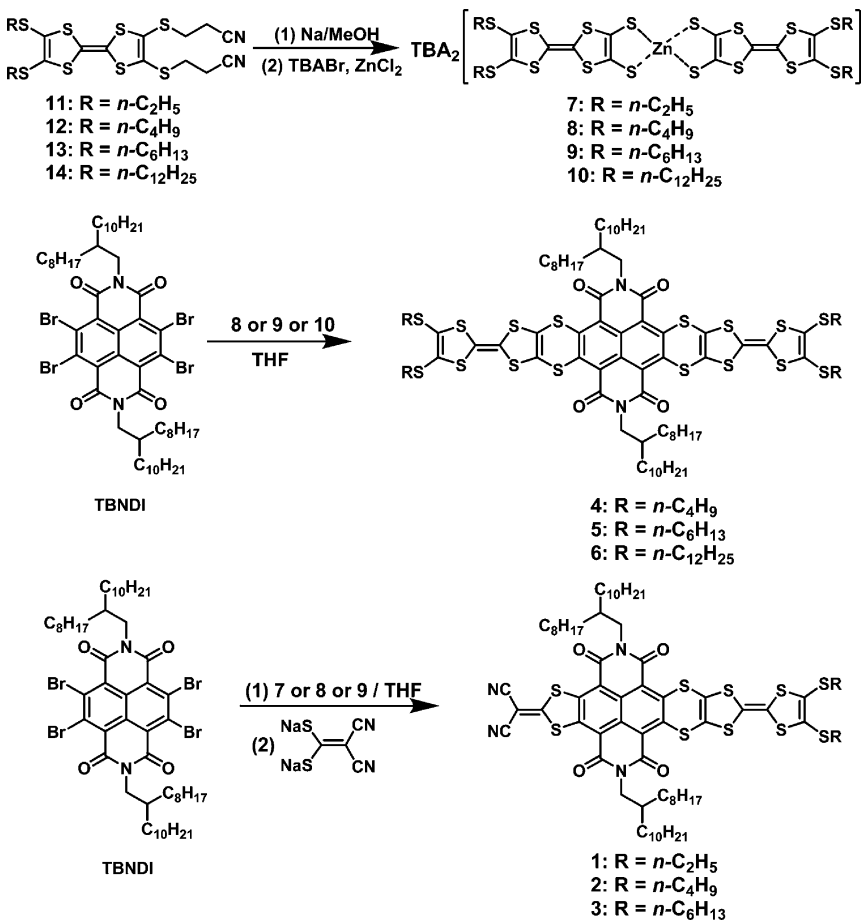

Scheme 1 Synthetic approaches for compounds **1–6.**

Results and discussion

Synthesis and characterization

The synthetic approaches to compounds **1–6** are shown in Scheme 1. Removal of $-CH_2CH_2CN$ groups of compounds **11–14** with $NaOCH_3$ led to the corresponding sodium salts which were transformed to the respective zinc salts **7–10** according to the reported procedures.[42] Reaction of TBNDI (tetrabromonaphthalene diimide), which was prepared by bromination of naphthalene dianhydride and sequential condensation with 2-octydodecylamine according to the reported procedures,[43,44] with **8–10** separately at room temperature yielded compounds **4–6** in acceptable yields (see Experimental section). Note that the reaction of the corresponding sodium salts with TBNDI was rather complicated based on TLC analysis and compounds **4–6** could not be separated from the reaction mixtures.

Compounds **1–3** were prepared by first addition of the respective zinc salt (**7–9**) to the TBNDI solution, followed by addition of the sodium salt of 2-(1,3-dithiol-2-ylidene)malonitrile and stirring the reaction mixtures at room temperature for 1.0 h. After column chromatographic separation compounds **1–3** were obtained in acceptable yields. However, first addition of the sodium salt of 2-(1,3-dithiol-2-ylidene)malonitrile to TBNDI solution, followed by addition of the respective zinc salt, did not afford compounds **1–3**. This is probably due to the fact that 2-(1,3-dithiol-2-ylidene)malonitrile is electron withdrawing and as a result the connection of a 2-(1,3-dithiol-2-ylidene)malonitrile moiety to the NDI core would further activate the C–Br bonds; accordingly, the reaction in this condition mainly leads to symmetrically substituted NDI compounds with either two 2-(1,3-dithiol-2-ylidene)malonitrile or two TTF moieties.

The chemical structures and purities of compounds **1–6** were established and confirmed by spectroscopic data and elemental analysis (see Experimental section). Compounds **1–6** show good solubilities (>10 mg mL^{-1}) in common solvents such as CH_2Cl_2, $CHCl_3$, THF and dichlorobenzene. Based on TGA analysis (Fig. S1–S6, ESI†) compounds **1–6** are thermally stable below 230 °C.[45]

HOMO/LUMO energies and chemical structures

The redox potentials of compounds **1–6** were measured with cyclic voltammetry. As examples, Fig. 1 shows the cyclic voltammograms of **1** and **4**. For comparison, the redox potentials of *N*,*N*′-hexyl naphthalene diimides (*N*,*N*′-hexyl NDI) and **13** as reference compounds (see Fig. S12 and S13, ESI†) were also measured under the same conditions. As shown in Table 1, the oxidation potentials of **1–6** were positively shifted compared to compound **13**. This is likely due to the electron-withdrawing effect of NDI units in **4–6** and as a result their HOMO energies were lowered. For compounds **1–3**, besides the NDI units, 2-(1,3-dithiol-2-ylidene)malonitrile moieties may further induce the decrease of the HOMO energies. In fact, this is in agreement with the theoretical calculations as to be discussed below. However, the reduction potentials of **1–6** were positively shifted compared to *N*,*N*′-hexyl NDI (see Table 1). This can be understood by considering the fact the covalent connection of TTF to the NDI core may increase the conjugation degree of **1–6**; accordingly, the respective radical anions may become more stable.

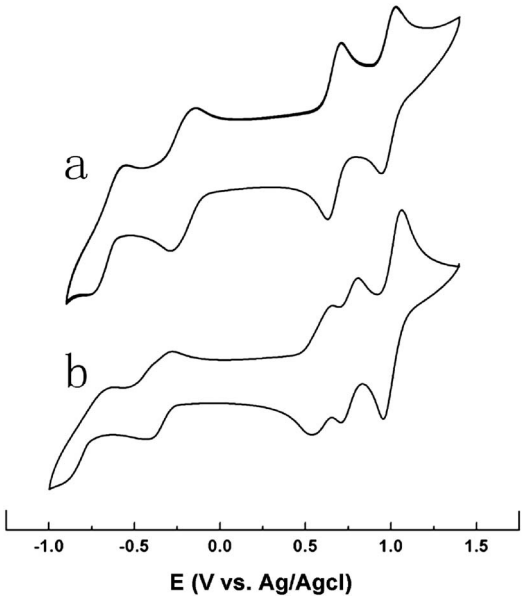

Fig. 1 Cyclic voltammograms of compounds **1** (a) and **4** (b) in CH_2Cl_2 solutions (1.0×10^{-3} M) at a scan rate of 100 mV s^{-1}, with Pt as the working and counter electrodes and Ag/AgCl electrode (saturated KCl) as the reference electrode, and *n*-Bu_4NPF_6 (0.1 M) as supporting electrolyte.

The HOMO/LUMO energies of **1–6** can be estimated based on their onset oxidation and reduction potentials (HOMO = E_{onset}^{ox1} − 4.4 eV, LUMO = − (E_{onset}^{red1} + 4.4) eV), according to previous reports.[46,47] As listed in Table 1, the HOMO energies of **4–6** (*ca.* −5.0 eV) are higher than those of **1–3** (*ca.* −5.1 eV), while the LUMO energies of **1–3** (*ca.* −4.3 eV) were lower than of **4–6** (*ca.* −4.1 eV). These agree with the fact that **4–6** contain two electron-donating TTF moieties, whereas **1–3** contain the electron withdrawing 2-(1,3-dithiol-2-ylidene)malonitrile moiety apart from one TTF moiety. The band gaps were deduced to be 0.8 and 0.9 eV for **1–3** and **4–6**, respectively, based on their HOMO/LUMO energies as listed in Table 1.

Compared to those of references compounds *N*,*N*′-hexyl NDI and **13**, **1–3** exhibit new absorptions around 550 nm and 840 nm (see Fig. 2 and Fig. S7–S9, ESI†). Similarly, new absorptions around 530 and 780 nm were detected for **4–6** compared to those of *N*,*N*′-hexyl NDI and **13** (see Fig. 2 and Fig. S7, S10 and S11, ESI†). The appearance of these new absorptions indicate the interactions between the TTF and NDI moieties within **4–6** and among the TTF, NDI and 2-(1,3-dithiol-2-ylidene)malonitrile moieties within **1–3**. Moreover, the absorptions of thin films of **1–6** were also measured (see Fig. 2 and Fig. S8–S11, ESI†). The absorption spectra of thin films of **1–6** were red-shifted compared to those in solutions: for **1–3** the absorption at 550 nm in solution was shifted to 620 nm and that at 840 was extended to the near-infrared region; similarly, the absorptions at 530 and 780 nm were shifted to 580 and 1400 nm, respectively, for **4–6**. Such absorption spectral shifts should be due to the intermolecular interactions within thin films of **1–6** which may include electron-donor–acceptor interactions.[48] Based on the absorption spectra

Table 1 Redox potentials and HOMO/LUMO energies of **1–6** and those of *N*,*N*′-hexyl NDI and **13**

Compound	$E_{1/2}^{red1}$/V	$E_{1/2}^{ox1}$/V	HOMO/eV	LUMO/eV	E_g^{CV}/eV
1	−0.22	0.65	−5.1	−4.3	0.8
2	−0.21	0.66			
3	−0.21	0.65			
4	−0.35	0.59	−5.0	−4.1	0.9
5	−0.34	0.58			
6	−0.50 (peak)	0.67 (peak)	−4.9	−4.0	0.9
NDI	−0.62				
13	—	0.51			

of their thin films, the band gaps of **1–3** and **4–6** were estimated to be 0.8 and 0.9 eV, respectively. These are in good agreement with those obtained with cyclic voltammetric data as mentioned above.

The chemical structures of **1–6** were investigated with theoretical calculations based on density functional theory (DFT). It is expected that the alkyl chains at the *N*,*N*′-positions of NDI cores and TTF moieties in **1–6** should not have a strong influence on the their electronic structures. Thus, the alkyl chains were replaced by methyl groups for the DFT calculations. As depicted in Fig. 3, the NDI core and the four bridging sulfur atoms are almost co-planar; the 2-(1,3-dithiol-2-ylidene)malonitrile groups in **4–6** are also co-planar with the NDI core. However, the TTF moieties in **1–3** and **4–6** are not co-planar with the respective NDI cores, forming dihedral angles of 133° and 135° with the NDI cores in **1–3** and **4–6**, respectively.

The theoretical calculations indicate that the HOMO orbitals of both **1–3** and **4–6** are localized on the respective TTF moieties (see Fig. 3). The LUMO orbitals of **1–3** reside mainly on the NDI core and the 2-(1,3-dithiol-2-ylidene)malonitrile moiety and those of **4–6** reside mostly on the NDI core. In addition, the four bridging sulfur atoms of **1–6** also make contributions to their LUMO orbitals (see Fig. 3). The HOMO energies of **1–3** and **4–6** were calculated to be −5.25 and −5.02 eV, respectively; LUMO energies of **1–3** and **4–6** were −4.03 and −3.62 eV, respectively. Accordingly, the band gaps of **1–3** and **4–6** were estimated to be 1.22 and 1.40 eV, respectively.

The solvent effects were not included in the theoretical calculations and thus there were differences between the LUMO and HOMO energies calculated theoretically and those obtained based on the electrochemical and spectroscopic data. However, data obtained from both methods indicate that LUMO energies of **1–3** are considerably lowered compared to that of the unsubstituted NDI (of which the LUMO energy was reported to be −3.8 eV);[49] as a result **1–3** may exhibit air-stable semiconducting behaviors in OFETs. Moreover, both **4–6** and **1–3** possess very narrow band gaps of less than 1.8 eV, and they are potentially ambipolar semiconductors according to previous reports.[50]

OFETs based on thin films of 1–3 and 4–6

Thin films of **1–6** were prepared by spin-coating for the fabrication of OFETs. A heavily doped Si wafer and a layer of dry oxidized SiO_2 (300 nm) were used as a gate electrode and gate dielectric layer, respectively. The drain–source (D–S) gold contacts were fabricated by photolithography; the D and S electrodes were further modified with pentafluorobenzenethiol for a better surface contact between electrode and semiconductors (see Experimental section).[51] The annealing processes were carried out in vacuum condition for 1.0 h at each temperature. The corresponding transfer characteristics and output characteristics of OFETs were measured under ambient conditions. Based on *I*–*V* curves of such measurements, the key characteristics of OEFTs were obtained.

As an example, Fig. 4 depicts the *I*–*V* curves of the OFETs with thin films of **3**. Interestingly, I_{DS} increased eventually by applying either positive or negative gate voltages (V_{GS}). The transfer *I*–*V* curves exhibit a 'V' shape which is characteristic for ambipolar OFETs. Similar transfer characteristics were also observed for OFETs with thin films of either **1** or **2**. These results

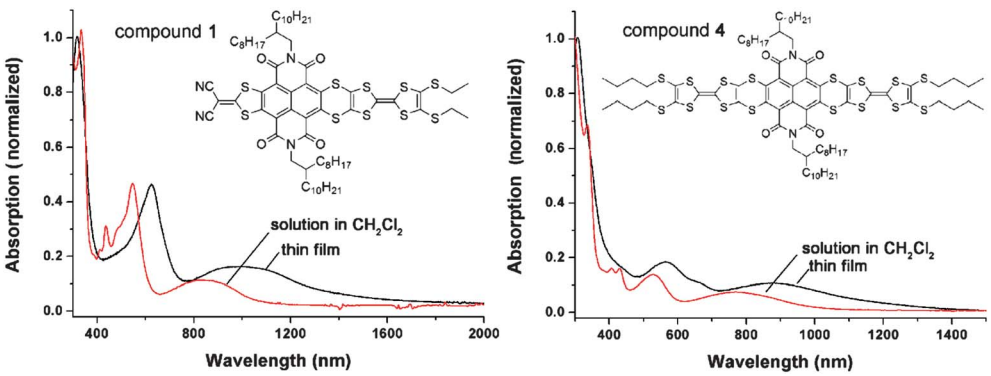

Fig. 2 Absorption spectra of compounds **1** (left) and **4** (right) in solution ($\varepsilon_{550nm} = 1.0 \times 10^4$ M^{-1} cm^{-1} for **1** and $\varepsilon_{530nm} = 8.6 \times 10^3$ M^{-1} cm^{-1} for **4** in CH_2Cl_2) and thin films.

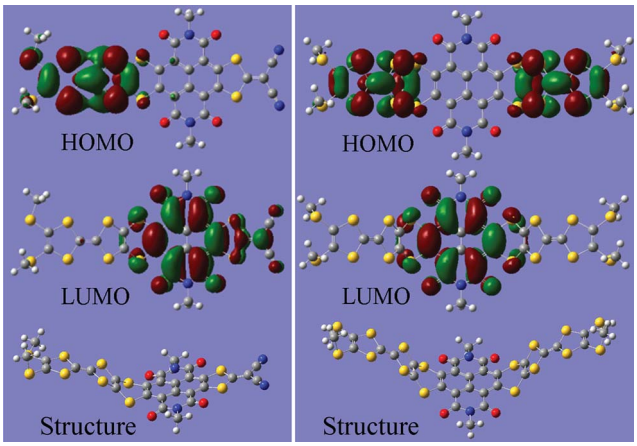

Fig. 3 HOMO, LUMO orbitals and structures of compounds **1–3** (left) and **4–6** (right) obtained by DFT calculations; the alkyl chains were replaced by methyl groups in the calculations (see ESI†).

demonstrate that compounds **1–3** exhibit ambipolar semiconducting behaviors.

The hole (μ_h) and electron mobilities (μ_e) of the as-prepared OFETs based on **1** were measured to be 1.2×10^{-5} and 3.1×10^{-5} cm^2 V^{-1} s^{-1} at room temperature, respectively; moreover, both μ_h and μ_e were enhanced by annealing the thin films of **1** at different temperatures as shown in Table 2. For instance, the OFETs based on **1** showed μ_h and μ_e of 3.0×10^{-4} and 1.1×10^{-4} cm^2 V^{-1} s^{-1}, respectively, after annealing at 160 °C. The as-prepared OFETs with thin films of **2** exhibited μ_h and μ_e of 1.2×10^{-4} and 3.1×10^{-5} cm^2 V^{-1} s^{-1}, respectively; both μ_h and μ_e increased slightly after annealing (see Table 2). OFETs of **3** exhibited similar performances as those with **1** and **2**; μ_h and μ_e increased to 2.0×10^{-4} and 1.6×10^{-5} cm^2 V^{-1} s^{-1} after annealing at 120 °C and further to 2.3×10^{-4} and 7.2×10^{-5} cm^2 V^{-1} s^{-1}, respectively, after annealing at 140 °C. Interestingly, the hole and electron mobilities of OFETs with **3** reached 0.03 cm^2 V^{-1} s^{-1} and $\mu_e = 0.003$ cm^2 V^{-1} s^{-1}, respectively, after further annealing at 160 °C. This significant increase in μ_h and μ_e for OFETs of **3** is in agreement with the formation of interconnected large domains within the thin films of **3** as to be discussed below. After annealing at 160 °C, the OFETs of **3** were left in air up to ten days for stability tests. As depicted in Fig. 5, the hole mobility decreased to 83% after the first three days and then remained almost unaltered; the electron mobility decreased quickly for the first three days and then only slightly and it retained 71% of the initial value. These data reveal that the stability of OFETs based on **3** is acceptable. Note that efforts were also made to increase the hole and electron mobilities of OFETs with **1–3** by modification of the drain and source Au electrodes with pentafluorobenzenethiol. However, obvious increases of μ_h and μ_e were not achieved.

OFETs with thin films of **4–6** were fabricated with either Au or modified Au with pentafluorobenzenethiol as drain and source electrodes. The results manifest that OFETs with modified Au (with pentafluorobenzenethiol) as drain and source electrodes show higher performance compared to those with unmodified Au electrodes (see Table S1, ESI†). The data in Table 3 were obtained with the modified Au electrodes. Fig. 6 shows the transfer characteristics of the OFET with **5**; obviously, I_{DS} increased by applying the negative V_{GS}. Similar transfer characteristics were also observed with thin films of **4** and **6**. Thus, it can be concluded that compounds **4–6** behave as p-type semiconductors. The performance of OFETs with **4–6** was gradually improved after annealing at different temperatures. For instance, the as-prepared OFETs of **5** shows hole mobility (μ_h) of 0.0012 cm^2 V^{-1} s^{-1} and on/off ratio ($I_{on/off}$) of 10^3 which further increased to 0.07 cm^2 V^{-1} s^{-1} and 10^4, after annealing at 120 °C. Moreover, μ_h increased further to 0.15 cm^2 V^{-1} s^{-1} after annealing at 140 °C and reached the maximum ($\mu_h = 0.31$ cm^2 V^{-1} s^{-1}) after annealing at 160 °C. The hole mobilities of OFETs with **4** and **6** also became higher after annealing, reaching 0.007 and 0.11 cm^2 V^{-1} s^{-1}, respectively, after annealing at 160 and 120 °C (see Table 3). However, the performance of OFETs based on **6** was reduced after further increasing the annealing

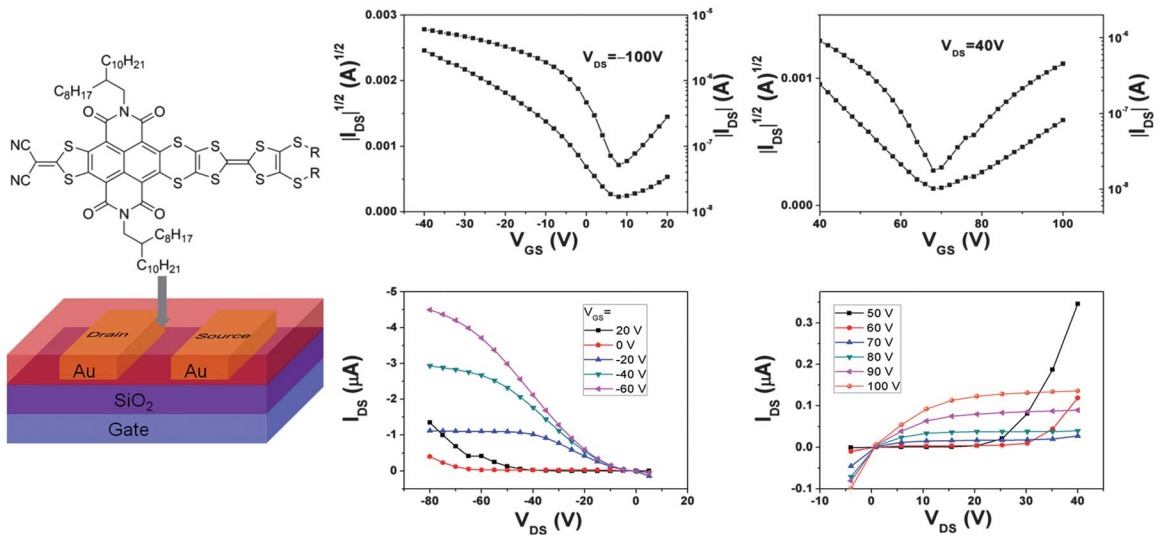

Fig. 4 Device structure, transfer and output characteristics for OFETs with **3** after annealing at 160 °C; the channel width (W) and length (L) were 1440 μm and 40 μm, respectively.

Table 2 The hole and electron mobilities (μ_h and μ_e), threshold voltages (V_{th}) for bottom contact OFET devices based on thin films of **1–3** at different annealing temperatures[a]

Compound	T/°C	μ_h/cm^2 V^{-1} s^{-1}	μ_e/cm^2 V^{-1} s^{-1}	V_{th}/V	
				p	n
1	25	(0.9–1.2) × 10^{-5}	(2.4–3.1) × 10^{-5}	−27 to −25	10 to 13
	120	(2.0–2.4) × 10^{-4}	(0.8–1.1) × 10^{-4}	−30 to −26	20 to 24
	140	(2.2–2.4) × 10^{-4}	(0.9–1.1) × 10^{-4}	−27 to −26	15 to 17
	160	(2.5–3.0) × 10^{-4}	(0.9–1.1) × 10^{-4}	−25 to −20	24 to 26
2	25	(0.8–1.2) × 10^{-4}	(2.7–3.1) × 10^{-5}	−36 to −34	13 to 17
	120	(2.0–2.7) × 10^{-4}	(4.8–5.3) × 10^{-5}	−29 to −26	10 to 16
	140	(4.0–4.2) × 10^{-4}	(5.1–5.4) × 10^{-5}	−35 to −30	−5 to −7
	160	(4.5–5.3) × 10^{-4}	(7.1–7.5) × 10^{-5}	−29 to −26	−7 to −10
3	25	(1.9–2.4) × 10^{-5}	(0.8–1.0) × 10^{-5}	−27 to −25	8 to 15
	120	(1.7–2.0) × 10^{-4}	(1.4–1.6) × 10^{-5}	−28 to −20	16 to 20
	140	(1.9–2.3) × 10^{-4}	(6.4–7.2) × 10^{-5}	−27 to −20	15 to 27
	160	0.01–0.03	0.001–0.003	−10 to −5	50 to 70

[a] The performance data were obtained based on more than 10 different OFET devices. Because the devices could not be shut down completely, the on/off ratios were unable to be determined.

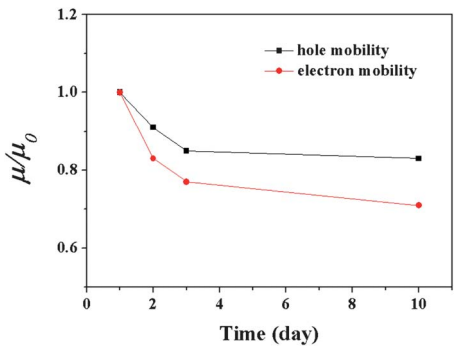

Fig. 5 Variation of the hole and electron mobilities for OFET devices of **3** left in air for 10 days.

Table 3 The hole mobilities (μ_e), threshold voltages (V_{th}), and on/off ratios ($I_{on/off}$) for bottom contact OFET devices based on thin films of **4–6** at different annealing temperatures[a]

Compound	T/°C	μ_h/cm^2 V^{-1} s^{-1}	V_{th}/V	$I_{on/off}$
4	25	(3.8–4.2) × 10^{-4}	−5 to 0	10^2
	120	(0.9–1.0) × 10^{-3}	−6 to 2	10^2
	140	(1.5–2.0) × 10^{-3}	−5 to 3	10^3
	160	(5.0–7.0) × 10^{-3}	−3 to 1	10^3
5	25	(0.8–1.2) × 10^{-3}	0 to 7	10^3
	120	0.05–0.07	5 to 10	10^4
	140	0.10–0.15	−5 to −7	10^4
	160	0.17–0.31	−5 to 6	10^4
6	25	(5.9–7.8) × 10^{-4}	−1 to 0	10^2
	100	0.03–0.05	−4 to 5	10^4
	120	0.09–0.11	0 to 5	10^4
	140	0.06–0.07	−5 to −3	10^4

[a] The performance data were obtained based on more than 10 different OFET devices.

temperatures. The stabilities of OFETs based on **4–6** were also examined. As an example, Fig. 7 shows the variation of the hole mobility and on/off ratio after the OFETs of **5** were left in air up to ten days. The hole mobility reduced to its 81% on the tenth day while the on/off ratio remain almost unchanged. Thus, OFETs based on **4–6** exhibit good stability.

Compounds **1–3** possess the same conjugated framework but they contain different alkyl chains within the TTF moieties. The same holds true for compounds **4–6**. The studies based OFETs reveal that **3** exhibits good ambipolar semiconducting property in terms of high hole and electron mobilities in comparison with **1** and **2**, and thin films of **5** shows highest hole mobility after annealing among compounds **4–6**. As to be discussed below these alkyl chains may affect the intermolecular packing of the conjugated frameworks, and as a result the corresponding transporting behaviors of **1–6** may be influenced by the features of alkyl chains. Alternatively, these results also show that it is possible to tune the semiconducting properties of conjugated molecules by varying the alkyl chains that are covalently connected to the conjugated cores.

XRD and AFM studies

Thin films of **1–6** deposited on the OTS-modified SiO_2 substrates were investigated with XRD (X-ray diffraction) and AFM (atomic force microscopy), in order to understand the variation of their semiconducting behaviors upon annealing. Fig. 8 shows the XRD pattern of an as-prepared thin film of **3** at 25 °C and those after annealing at 120, 140 and 160 °C. Weak diffraction peaks at 4.3, 8.6, 11.8, 21.2, 23.6 and 26.4° were detected for the as-prepared thin film of **3**. After annealing at 140 °C, the peak intensities at 4.3 and 8.6° were largely enhanced. After annealing at 160 °C, the peak intensity at 4.3° increased further, whereas other diffraction peaks still remain; however, a new diffraction peak at 3.6° with high intensity and a weak one at 7.2° emerged after annealing at 160 °C. The exact intermolecular packing for **3** cannot be deduced based on these XRD data; but the enhancement of diffraction peak intensities and appearance of new diffraction peaks do indicate that molecules of **3** are arranged in a more orderly manner within the thin film and crystallinity is improved after annealing at higher temperatures. Intermolecular

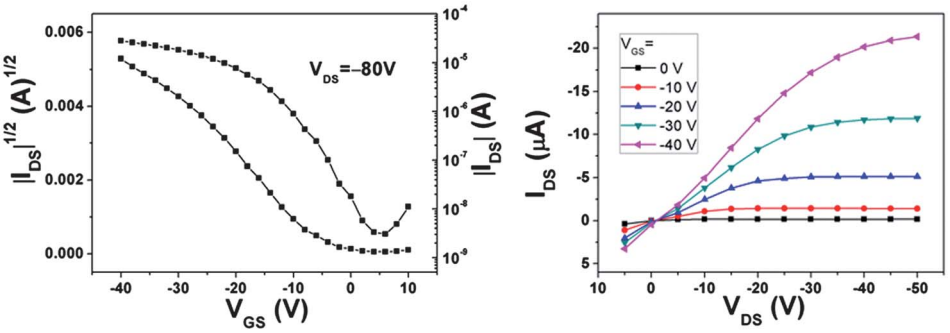

Fig. 6 Transfer and output characteristics for OFET of **5** after annealing at 160 °C; the channel width (*W*) and length (*L*) were 1440 μm and 50 μm, respectively.

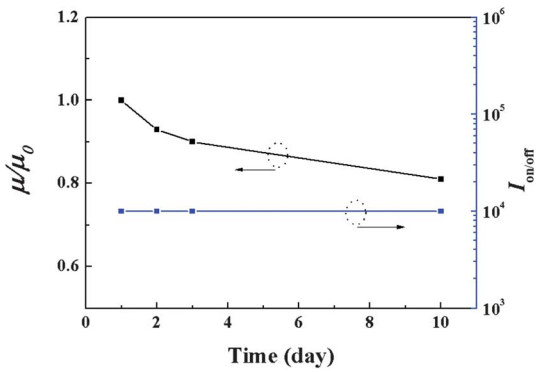

Fig. 7 Variation of the hole mobility and on/off ratio for OFET devices of **5** left in air for 10 days.

ordered packing is known to be beneficial for the improvement of the carrier mobilities of organic semiconductors, and this is indeed consistent with the mobility data (see Table 2) for thin films of **3** after annealing at different temperatures.

The as-prepared thin film of **3** entailed stripes of different sizes as indicated by the AFM image shown in Fig. 8. After annealing at 120 °C the stripes became larger and more interconnected. Similar morphological changes were observed after annealing at 140 °C. Interestingly, the stripes merged to form large and continuous domains after annealing at 160 °C (see Fig. 8). Such significant morphology variation is coincident with the obvious change of XRD pattern after annealing the thin film at 160 °C. Moreover, the formation of large domains is again in agreement with the high carrier mobility of the thin film of **3**.[52]

The XRD patterns and AFM images of thin films of analogous compounds **1** and **2** were also measured after annealing at different temperatures (see Fig. S18 and S19, ESI†). Similarly, a diffraction peak at *ca.* 4.3° became strong and new diffraction peaks appeared after annealing. However, compared to that for thin film of **3** the diffraction patterns for thin films of **1** and **2** were not significantly enhanced after annealing at 160 °C. Importantly, AFM images also revealed that large and continuous domains were not formed for thin films of **1** and **2** after annealing even at 160 °C. These investigations agree well with the fact that mobilities of thin films of **1** and **2** are comparably lower than those of **3** (see Table 2).

Fig. 9 depicts the XRD patterns of a thin film of **5** after annealing at different temperatures and that of the as-prepared thin film. Only weak diffraction peaks at 21.2 and 23.6° were detected for the as-prepared thin film of **5**. However, a new diffraction peak with high intensity at 3.6° and weak peaks at 7.2, 11.8 and 26.4° appeared after annealing at 120 °C. The XRD pattern remains almost unaltered after annealing at either 140 or 160 °C with only slight intensity enhancement for the diffraction peak at 3.6°. AFM images indicated large domains were formed after annealing at 120 °C, and further annealing at 140 and 160 °C led to slight increase of the domain sizes. These XRD and AFM data are in good agreement with the fact that OFET performances of thin films of **5** are improved after annealing (see Table 3).

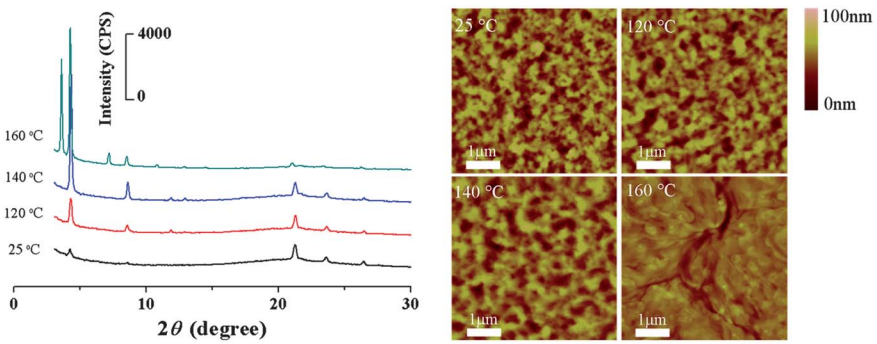

Fig. 8 XRD patterns (left) and AFM images (right, on OTS modified Si substrate with tapping mode) of a thin film of **3** after annealing at different temperatures.

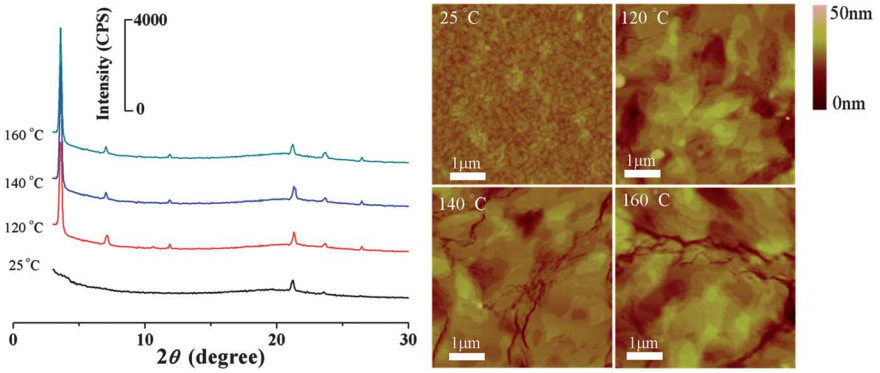

Fig. 9 XRD patterns (left) and AFM images (right, on OTS modified Si substrate with tapping mode) of a thin film of **5** after annealing at different temperatures.

The XRD patterns and AFM images of the analogous compounds **4** and **6** were also measured (see Fig. S20 and S21, ESI†). Similarly, a new diffraction peak with high intensity and additional weak diffraction signals emerged for thin films of **4** and **6** after annealing at high temperatures. Such changes in the XRD pattern also show that molecules of either **4** or **6** are more ordered in the respective thin films after annealing. This is again in agreement with the enhancement of carrier mobilities for thin films of **4** or **6** after annealing (see Table 3). The thin film morphologies of thin films of **4** or **6** were also modified after annealing based on the corresponding AFM images shown in Fig. S20 and S21 (ESI†). For instance, rod-like structures with sizes of *ca.* 0.4 μm × 0.1 μm and *ca.* 0.8 μm × 0.2 μm (see Fig. S20, ESI†) were formed for a thin film of **4** after annealing at 140 and 160 °C, respectively. However, these rod-like structures were not transformed into large domains for thin films of **4** after annealing at high temperatures. For the thin film of **6** the grain size increased obviously after annealing, but grain boundaries were formed simultaneously. Accordingly, these morphological differences between thin film of **5** and those of **4/6** may provide an explanation for their differences in semiconducting properties in terms of carrier mobilities (see Table 3) after annealing.

As discussed above, compounds **4–6** have the same conjugated framework with four alkyl chains of different lengths (*n*-C_4H_9, *n*-C_6H_{13} and *n*-$C_{12}H_{25}$) linked to TTF moieties. From **4** to **5**, the alkyl chains were simply lengthened by two carbon atoms, but the hole and electron mobilities of **5** were obviously higher than those of **4** (see Table 3). However, further extending the lengths of alkyl chains to –$C_{12}H_{25}$ in **6** led to the reduction of the hole and electron mobilities. Close examination of the XRD diffraction patterns of thin films of **4–6** (Fig. 9 and Fig. S20, S21, ESI†) reveal that they exhibit typical lamellar structures because of the presence of integral multiplied diffraction peaks. For instance, diffraction peaks were detected at 3.7 and 7.4° for the thin film of **4**, at 3.6 and 7.2° for the thin film of **5**, and at 2.9, 5.6 and 8.4° for the thin film of **6** after annealing at 120 °C, as depicted in Fig. 10. Accordingly, the *d*-spacing for the lamellar structures increases by extending the lengths of alkyl chains from **4** to **6**.[53] Thus, it may be concluded that such lamellar structures are dictated by the interactions among alkyl chains linked to TTF moieties rather than the alkyl chains at *N*,*N*′-positions of NDI core, as illustrated in Fig. 10. In addition, thin films of **4–6** showed diffraction peaks around 21.2, 23.6 and 26.4°, corresponding to *d*-spacings of 4.1, 3.7 and 3.4 Å, respectively. These short *d*-spacings may indicate the intermolecular interactions of conjugated frameworks in **4–6** which may contain intermolecular π–π, electron donor–acceptor and S···S interactions.

In comparison, all thin films of **1–3** exhibited diffraction peaks at 4.3 and 8.6° after annealing at 120 and 140 °C (see Fig. 8 and Fig. S18, S19, ESI†). Fig. 10 collects the XRD patterns of thin films of **1–3** after annealing at 140 °C. These XRD data indicate that thin films of **1–3** possess similar lamellar structures and the corresponding *d*-spacing is not affected by the alkyl chains linking to TTF moieties.[54] Therefore, such lamellar structures may be determined by the interactions among alkyl chains at *N*,*N*′-positions as schematically illustrated in Fig. 10. Even after annealing at 160 °C the XRD patterns remained almost unaltered for thin films of **1** and **2** (see Fig. S18 and S19, ESI†). However, new diffraction peaks at 3.6 and 7.2° emerged for a thin film of **3** after annealing at 160 °C as shown in Fig. 10. Of note are that these two XRD signals are the same as those for a thin film of **5**; moreover, as for **5** compound **3** also possesses two *n*-C_6H_{13} chains. Thus, another lamellar structure, which should be similar to those within thin films of **4–6** dictated by the alkyl chains with TTF moieties, appeared for a thin film of **3**. As a result, it may be concluded that two lamellar structures co-existed within a thin film of **3** after annealing at 160 °C. Such structural change may affect the intermolecular interactions of the conjugated core in **3** and the formation of large domains which are beneficial for the enhancement of carrier mobilities. Similarly, the diffraction peaks around 21.2, 23.6 and 26.4° reflect the intermolecular π–π, electron donor–acceptor and S···S interactions.

It is still challenging to understand the correlation between the chemical structures and the carrier mobilities at this stage. However, current studies with **4–6** as well as **1–3** and previous reports[41] do indicate that it is possible to tune the semiconducting behaviors of organic conjugated molecules by altering the alkyl chains attached to the conjugated cores.

Conclusions

With the motivation to tune the HOMO/LUMO energies and thus develop new organic semiconductors, in particular

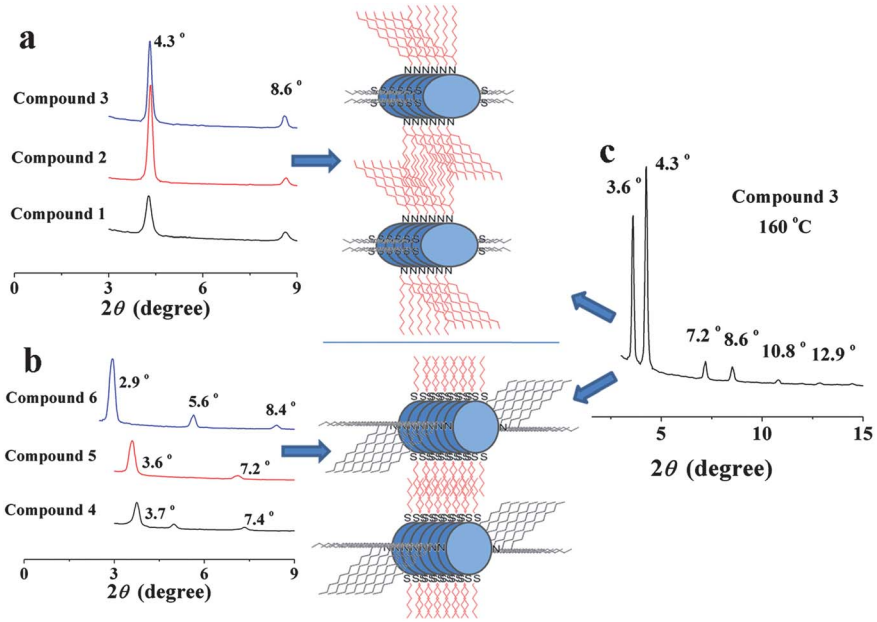

Fig. 10 (a) XRD patterns of **1–3** annealed at 140 °C; (b) XRD patterns of **4–6** annealed at 120 °C; (c) XRD patterns of **3** annealed at 160 °C; the intensities of diffraction peaks were slightly altered for a better view; illustration of the corresponding lamellar structures dictated by interactions of different alkyl chains.

ambipolar semiconductors, core-expanded NDI compounds fused with two TTF moieties (**4–6**) and both TTF and 2-(1,3-dithiol-2-ylidene)malonitrile moieties (**1–3**) were synthesized and investigated. Cyclic voltammetric and absorption spectral studies reveal that **1–6** posses a narrow band gap of *ca.* 0.9 eV and their HOMO/LUMO energies can be tuned by linking TTF (as electron donor) and 2-(1,3-dithiol-2-ylidene)malonitrile (as electron acceptor) to the NDI core. Compounds **1–6** are solution-processible and thin films can be easily prepared with spin-coating techniques. Of interest is the finding that **1–3** exhibit ambipolar semiconducting properties and **4–6** behave as p-type semiconductors based on OFET studies. Moreover, their carrier mobilities in air increased after further annealing; among **1–3**, thin films of **3** exhibit relatively high hole and electron mobilities in air, reaching 0.03 and 0.003 $cm^2\ V^{-1}\ s^{-1}$, respectively, after annealing at 160 °C. Note that these hole and electron mobilities are among the best performances (in air) of ambipolar semiconductors reported;[26] the OFETs with thin films of **5** show the best performance with $\mu_h = 0.31\ cm^2\ V^{-1}\ s^{-1}$, $I_{on/off} = 10^4$ among compounds **4–6** after annealing at 160 °C. Compounds **4–6** are new p-type semiconductors based on an NDI core and also exhibit relatively high hole mobilities compared to TTF-based OFETs prepared by a solution process.[41] Both XRD and AFM studies show that intermolecular arrangement and morphological changes occurred for thin films of **1–6** after annealing. These agree well with the variation of the performances of the corresponding OFETs. The results of the current research clearly demonstrate that (1) conjugated electron donor–acceptor frameworks are appealing for designing new organic semiconductors, in particular ambipolar semiconductors, by tuning the HOMO/LUMO energies and intermolecular interactions; (2) alkyl chains can significantly affect the intermolecular arrangements of conjugated molecular cores and hence the respective semiconducting properties.

Experimental section

Fabrication of OFET devices

Bottom contact OFETs were fabricated. A heavily doped n-type Si wafer and a layer of dry oxidized SiO_2 (300 nm) were used as a gate electrode and gate dielectric layer, respectively. The drain–source (D–S) gold contacts were fabricated by photolithography. The substrates were cleaned in water, deionized water, alcohol and rinsed in acetone. Then, the surface was modified with *n*-octadecyltrimethoxysilane (OTS). After that, the substrates were cleaned in *n*-hexane and $CHCl_3$, followed by soaking in 50 ml of EtOH to which 50 μL of pentafluorobenzenethiol was added. After 30–60 min the substrates were washed with EtOH. Compounds **1–6** were dissolved in $CHCl_3$ (about 10 mg mL^{-1}) and spin-coated on the substrate at 2500 rpm. The annealing process was carried out in vacuum for 1.0 h at each temperature.

The mobility of the OFETs in the saturation region was extracted from eqn (1):

$$I_{DS} = \frac{W}{2L}\mu C_i(V_{GS} - V_{th})^2 \quad (1)$$

where I_{DS} is the drain electrode collected current; L and W are the channel length and width, respectively; μ is the mobility of the device; C_i is the capacitance per unit area of the gate dielectric layer; V_{GS} is the gate voltage, and V_{th} is the threshold voltage. The V_{th} of the device was determined by extrapolating the $(I_{DS,sat})^{1/2}$ *vs.* V_{GS} plot to $I_{DS} = 0$.

TBNDI, compounds **11–14** and sodium 1,1-dicyanoethylene-2,2-dithiolate were synthesized according to the reported procedures.[55,56] Compound **7** were also synthesized according to the previous report[42] and **8–10** were obtained through the same method and the crude compounds were used without further purification.

Synthesis of 1

TBNDI (300 mg, 0.26 mmol) was dissolved in 50 mL THF and compound **7** (220 mg, 0.19 mmol) was added. After stirring at room temperature for 1.0 h, sodium 1,1-dicyanoethylene-2,2-dithiolate (72 mg, 0.39 mmol) was added and the mixture was stirred for 3.0 h. After that the mixture was diluted with water and extracted with CH_2Cl_2. The organic layer was dried with $MgSO_4$ and concentrated by rotary evaporation. The residue was purified by flash chromatography through a silica gel column with petroleum ether–CH_2Cl_2 (1 : 1, v/v) as eluent. The crude product was then dissolved in CH_2Cl_2 and re-precipitated by adding EtOH to give 90 mg (26% yield based on TBNDI) of **1** as a dark blue solid. ^{1}H NMR (400 MHz, $CDCl_3$) δ 4.20 (d, $J = 5.9$ Hz, 4H), 2.83 (br, 4H), 2.02 (br, 2H), 1.51–1.26 (m, 70H), 0.86 (br, 12H); ^{13}C NMR (150 MHz, CD_2Cl_2): δ 182.8, 161.8, 161.5, 144.8, 143.5, 127.6, 125.1, 120.7, 119.7, 117.4, 117.3, 111.9, 106.5, 69.6, 45.7, 36.5, 31.8, 31.3, 30.2, 29.6, 29.5, 29.2, 26.1, 22.5, 14.6, 13.77, 13.74; MS (MALDI-TOF): 1348.5 (M^+); Elemental analysis: calc. for $C_{68}H_{92}N_4O_4S_{10}$: C, 60.49; H, 6.87; N, 4.15; S, 23.75; found: C, 60.37; H, 6.90; N, 4.20; S, 23.53%.

Synthesis of 2

Compound **2** was synthesized similarly using compound TBNDI, **8** and sodium 1,1-dicyanoethylene-2,2-dithiolate. Compound **2** was obtained as a dark blue solid in 29% yield (based on TBNDI). ^{1}H NMR (600 MHz, CD_2Cl_2): δ 4.22 (br, 4H), 2.80 (br, 4H), 2.10 (br, 2H), 1.59 (br, 4H), 1.51–1.27 (m, 68H), 0.94 (br, 18H); ^{13}C NMR (150 MHz, CD_2Cl_2): δ 182.6, 161.8, 161.5, 144.2, 143.5, 127.4, 125.1, 120.6, 119.2, 117.38, 116.6, 111.8, 106.1, 69.5, 45.7, 36.5, 35.8, 31.8, 31.5, 31.3, 30.0, 29.59, 29.56, 29.2, 26.13, 26.09, 22.5, 21.4, 13.79, 13.75, 13.2; MS (MALDI-TOF): 1404.6 (M^+); Elemental analysis: calc. for $C_{72}H_{100}N_4O_4S_{10}$: C, 61.50; H, 7.17; N, 3.98; S, 22.80; found: C, 61.30; H, 7.21; N, 3.99; S, 22.88%.

Synthesis of 3

Compound **3** was synthesized similarly using compound TBNDI, **9** and sodium 1,1-dicyanoethylene-2,2-dithiolate. Compound **3** was obtained as a dark blue solid in 35% yield (based on TBNDI). ^{1}H NMR (600 MHz, CD_2Cl_2) δ 4.23 (br, 4H), 2.78 (br, 4H), 2.09 (br, 2H), 1.55 (br, 4H), 1.51–1.32 (m, 76H), 0.92 (br, 18H); ^{13}C NMR, (150 MHz, CD_2Cl_2) δ 182.7, 161.8, 161.5, 144.6, 143.4, 127.4, 125.1, 120.7, 119.6, 117.4, 116.8, 111.8, 106.8, 69.5, 45.7, 36.5, 36.2, 31.8, 31.3, 31.1, 30.05, 29.58, 29.55, 29.48, 29.2, 28.03, 26.1, 26.0, 22.5, 22.3, 13.78, 13.74, 13.6; MS (MALDI-TOF): 1460.6 (M^+); Elemental analysis: calc. for $C_{76}H_{108}N_4O_4S_{10}$: C, 62.42; H, 7.44; N, 3.83; S, 21.93; found: C, 62.53; H, 7.49; N, 4.01; S, 22.10%.

Synthesis of 4

TBNDI (300 mg, 0.26 mmol) was dissolved in 50 mL THF and compound **8** (490 mg, 0.39 mmol) was added. The mixture was stirred at room temperature for 3.0 h. After that the mixture was diluted with water and extracted with CH_2Cl_2. The organic layer was dried with $MgSO_4$ and concentrated by rotary evaporation. The residue was purified by flash chromatography through a silica gel column with petroleum ether–CH_2Cl_2 (3 : 1, v/v) as eluent. The crude product was then dissolved in CH_2Cl_2 and re-precipitated by adding EtOH to give 156 mg (35% yield based on TBNDI) of **1** as a dark purple solid. ^{1}H NMR (600 MHz, CD_2Cl_2) δ 4.13 (d, $J = 7.4$ Hz, 4H), 2.82 (br, 8H), 1.98 (br, 2H), 1.62–1.58 (m, 8H), 1.48–1.33 (m, 72H), 0.96–0.91 (m, 24H); ^{13}C NMR (150 MHz, CD_2Cl_2): δ 161.7, 144.6, 127.5, 123.5, 121.4, 121.2, 45.6, 36.5, 35.9, 31.9, 31.6, 31.5, 30.1, 29.6, 29.4, 29.3, 26.2, 22.7, 22.6, 21.6, 13.9, 13.8, 13.3; MS (MALDI-TOF): 1706.4 (M^+): Elemental analysis: calc. for $C_{82}H_{118}N_2O_4S_{16}$: C, 57.63; H, 6.96; N, 1.64; S, 30.02; found: C, 57.57; H, 6.98; N, 1.78; S, 30.02%.

Synthesis of 5

Compound **5** was synthesized similarly using compound TBNDI and **9**. Compound **5** was obtained as a dark purple solid in 37% yield (based on TBNDI). ^{1}H NMR (600 MHz, CD_2Cl_2): δ 4.13 (d, $J = 7.4$ Hz, 4H), 2.82 (br, 8H), 1.98 (br, 2H), 1.65–1.60 (m, 8H), 1.44–1.31 (m, 88H), 0.94–0.90 (m, 24H); ^{13}C NMR (150 MHz, $CDCl_3$) δ 162.7, 146.0, 128.5, 124.6, 122.5, 122.2, 119.7, 46.6, 37.4, 37.1, 32.8, 32.1, 31.0, 30.5, 30.2, 29.1, 27.1, 23.5, 23.3, 15.04, 15.00, 14.8; MS (MALDI-TOF): 1819.5 (M^+); Elemental analysis: calc. for $C_{90}H_{134}N_2O_4S_{16}$: C, 59.36; H, 7.42; N, 1.54; S, 28.17; found: C, 59.34; H, 7.50; N, 1.63; S, 27.87%.

Synthesis of 6

Compound **6** was synthesized similarly using compound TBNDI and **10**. Compound **6** was obtained a dark purple solid in 33% yield (based on TBNDI). ^{1}H NMR (600 MHz, CD_2Cl_2): δ 4.14 (br, 4H), 2.82 (br, 8H), 1.99 (br, 2H), 1.63 (br, 8H), 1.43–1.32 (m, 136H), 0.92 (br, 24H). ^{13}C NMR (150 MHz, CD_2Cl_2): δ 161.7, 144.8, 127.7, 123.5, 121.6, 121.3, 45.6, 36.5, 36.2, 31.9, 31.8, 31.5, 30.1, 29.65, 29.62, 29.5, 29.4, 29.36, 29.32, 29.1, 28.5, 26.2, 22.7, 22.6, 13.96, 13.89, 13.83; MS (MALDI-TOF): 2155.9 (M^+); Elemental analysis: calc. for $C_{114}H_{182}N_2O_4S_{16}$: C, 63.46; H, 8.50; N, 1.30; S, 23.78; found: C, 63.52; H, 8.61; N, 1.40; S, 23.87%.

Acknowledgements

The present research was financially supported by NSFC, the State Basic Program and Chinese Academy of Sciences. This work was partially supported by the NSFC-DFG joint project (TRR61). The authors thank the anonymous referees for the comments and suggestions which enabled us to further improve the manuscript.

Notes and references

1 J. E. Anthony, A. Facchetti, M. Heeney, S. R. Marder and X. Zhan, *Adv. Mater.*, 2010, **22**, 3876.
2 H. Klauk, U. Zschieschang, J. Pflaum and M. Halik, *Nature*, 2007, **445**, 745; H. Klauk, *Chem. Soc. Rev.*, 2010, **39**, 2643.
3 A. R. Murphy and J. M. J. Fréchet, *Chem. Rev.*, 2007, **107**, 1066; P. M. Beaujuge and J. M. J. Fréchet, *J. Am. Chem. Soc.*, 2011, **133**, 20009.
4 J. Zaumseil and H. Sirringhaus, *Chem. Rev.*, 2007, **107**, 1296.
5 C. Di, Y. Liu, G. Yu and D. Zhu, *Acc. Chem. Res.*, 2009, **42**, 1573.
6 R. Li, W. Hu, Y. Liu and D. Zhu, *Acc. Chem. Res.*, 2010, **43**, 529.
7 H. Dong, C. Wang and W. Hu, *Chem. Commun.*, 2010, **46**, 5211.
8 M. L. Tang, J. H. Oh, A. D. Reichardt and Z. Bao, *J. Am. Chem. Soc.*, 2009, **131**, 3733.

9 L. Li, Y. Zhang, H. Li, Q. Tang, L. Jiang, L. Chi, H. Fuchs and W. Hu, *Adv. Funct. Mater.*, 2009, **19**, 2987; L. Li, P. Gao, K. C. Schuermann, S. Ostendorp, W. Wang, C. Du, Y. Lei, H. Fuchs, L. D. Cola, K. Müllen and L. Chi, *J. Am. Chem. Soc.*, 2010, **132**, 8807.

10 Y. Cao, S. Liu, Q. Shen, K. Yan, P. Li, J. Xu, D. Yu, M. L. Steigerwald, C. Nuckolls, Z. Liu and X. Guo, *Adv. Funct. Mater.*, 2009, **19**, 2743; Y. Cao, M. L. Steigerwald, C. Nuckolls and X. Guo, *Adv. Mater.*, 2010, **22**, 20; S. S. Babu, S. Prasanthkumar and A. Ajayaghosh, *Angew. Chem., Int. Ed.*, 2012, **51**, 1766.

11 M. M. Payne, S. R. Parkin, J. E. Anthony, C. C. Kuo and T. N. Jackson, *J. Am. Chem. Soc.*, 2005, **127**, 4986; S. Subramanian, S. K. Park, S. R. Parkin, V. Podzorov, T. N. Jackson and J. E. Anthony, *J. Am. Chem. Soc.*, 2008, **130**, 2706; R. Hamilton, J. Smith, S. Ogier, M. Heeney, J. E. Anthony, I. McCulloch, J. Veres, D. D. C. Bradley and T. D. Anthopoulos, *Adv. Mater.*, 2009, **21**, 1166.

12 W. J. Liu, Y. Zhou, Y. G. Ma, Y. Cao, J. Wang and J. Pei, *Org. Lett.*, 2007, **9**, 4187; J. Y. Wang, Y. Zhou, J. Yan, L. Ding, Y. G. Ma, Y. Cao, J. Wang and J. Pei, *Chem. Mater.*, 2009, **21**, 2595; T. Lei, Y. Cao, Y. Fan, C.-J. Liu, S.-C. Yuan and J. Pei, *J. Am. Chem. Soc.*, 2011, **133**, 6099; S. Prasanthkumar, A. Saeki, S. Seki and A. Ajayaghosh, *J. Am. Chem. Soc.*, 2010, **132**, 8866; S. Prasanthkumar, A. Gopal and A. Ajayaghosh, *J. Am. Chem. Soc.*, 2010, **132**, 13206.

13 P. Gao, D. Beckmann, H. N. Tsao, X. L. Feng, V. Enkelmann, M. Baumgarten, W. Pisula and K. Müllen, *Adv. Mater.*, 2009, **21**, 213; X. Feng, V. Marcon, W. Pisula, M. R. Hansen, J. Kirkpatrick, F. Grozema, D. Andrienko, K. Kremer and K. Müllen, *Nat. Mater.*, 2009, **8**, 421; M. Zhang, H. N. Tsao, W. Pisula, C. Yang, A. K. Mishra and K. Müllen, *J. Am. Chem. Soc.*, 2007, **129**, 3472; H. N. Tsao, D. M. Cho, I. Park, M. R. Hansen, A. Mavrinskiy, D. Y. Yoon, R. Graf, W. Pisula, H. W. Spiess and K. Müllen, *J. Am. Chem. Soc.*, 2011, **133**, 2605.

14 T. Okamoto, M. L. Senatore, M. M. Ling, A. B. Mallik, M. L. Tang and Z. Bao, *Adv. Mater.*, 2007, **19**, 3381; J. Mei, D. H. Kim, A. L. Ayzner, M. F. Toney and Z. Bao, *J. Am. Chem. Soc.*, 2011, **133**, 20130.

15 Z. Wei, W. Hong, H. Geng, C. Wang, Y. Liu, R. Li, W. Xu, Z. Shuai, W. Hu, Q. Wang and D. Zhu, *Adv. Mater.*, 2010, **22**, 2458.

16 K. Takimiya, Y. Kunugi, Y. Toyoshima and T. Otsubo, *J. Am. Chem. Soc.*, 2005, **127**, 3605; I. Osaka, T. Abe, S. Shinamura and K. Takimiya, *J. Am. Chem. Soc.*, 2011, **133**, 6852; H. Ebata, T. Izawa, E. Miyazaki, K. Takimiya, M. Ikeda, H. Kuwabara and T. Yui, *J. Am. Chem. Soc.*, 2007, **129**, 15732; K. Takimiya, H. Ebata, K. Sakamoto, T. Izawa, T. Otsubo and Y. Kunugi, *J. Am. Chem. Soc.*, 2006, **128**, 12604; I. Osaka, T. Abe, S. Shinamura, E. Miyazaki and K. Takimiya, *J. Am. Chem. Soc.*, 2010, **132**, 5000.

17 L.-L. Chua, J. Zaumseil, J.-F. Chang, E. C.-W. Ou, P. K.-H. Ho, H. Sirringhaus and R. H. Friend, *Nature*, 2005, **434**, 194.

18 H. E. Katz, A. J. Lovinger, J. Johnson, C. Kloc, T. Siegrist, W. Li, Y. Y. Lin and A. Dodabalapur, *Nature*, 2000, **404**, 478.

19 B. A. Jones, M. J. Ahrens, M. H. Yoon, A. Facchetti, T. J. Marks and M. R. Wasielewski, *Angew. Chem., Int. Ed.*, 2004, **43**, 6363; B. A. Jones, A. Facchetti, M. R. Wasielewski and T. J. Marks, *J. Am. Chem. Soc.*, 2007, **129**, 15259.

20 F. Würthner and M. Stolte, *Chem. Commun.*, 2011, **47**, 5109; F. Würthner, *Angew. Chem., Int. Ed.*, 2001, **40**, 1037; R. Schmidt, M. M. Ling, J. H. Oh, M. Winkler, M. Könemann, Z. Bao and F. Würthner, *Adv. Mater.*, 2007, **19**, 3692; J. H. Oh, S.-L. Suraru, W.-Y. Lee, M. Könemann, H. W. Höffken, C. Röger, R. Schmidt, Y. Chung, W.-C. Chen, F. Würthner and Z. Bao, *Adv. Funct. Mater.*, 2010, **20**, 2148; R. D. Schmidt, J. H. Oh, Y.-S. Sun, M. Deppisch, A.-M. Krause, K. Radacki, H. Braunschweig, M. Könemann, P. Erk, Z. Bao and F. Würthner, *J. Am. Chem. Soc.*, 2009, **131**, 6215.

21 H. Yan, Z. H. Chen, Y. Zheng, C. Newman, J. R. Quinn, F. Dotz, M. Kastler and A. Facchetti, *Nature*, 2009, **457**, 679; Z. H. Chen, Y. Zheng, H. Yan and A. Facchetti, *J. Am. Chem. Soc.*, 2009, **131**, 8.

22 Z. Chen, H. Lemke, S. Albert-Seifried, M. Caironi, M. M. Nielsen, M. Heeney, W. Zhang, I. McCulloch and H. Sirringhaus, *Adv. Mater.*, 2010, **22**, 2371.

23 P. Sonar, S. P. Singh, Y. Li, M. S. Soh and A. Dodabalapur, *Adv. Mater.*, 2010, **22**, 5409.

24 A. R. Mohebbi, J. Yuen, J. Fan, C. Munoz, M. Wang, R. S. Shirazi, J. Seifter and F. Wudl, *Adv. Mater.*, 2011, **23**, 4644.

25 S. Cho, J. Lee, M. Tong, J. H. Seo and C. Yang, *Adv. Funct. Mater.*, 2011, **21**, 1910.

26 M. Irimia-Vladu, E. D. Głowacki, P. A. Troshin, G. Schwabegger, L. Leonat, D. K. Susarova, O. Krystal, M. Ullah, Y. Kanbur, M. A. Bodea, V. F. Razumov, H. Sitter, S. Bauer and N. S. Sariciftci, *Adv. Mater.*, 2012, **24**, 375.

27 J.-L. Brédas, J. Cornil, D. Beljonne, D. A. dos Santos and Z. Shuai, *Acc. Chem. Res.*, 1999, **32**, 267; C. R. Newman, C. D. Frisbie, D. A. da Silva Filho, J.-L. Brédas, P. C. Ewbank and K. R. Mann, *Chem. Mater.*, 2004, **16**, 4436.

28 X. Yang, L. Wang, C. Wang, W. Long and Z. Shuai, *Chem. Mater.*, 2008, **20**, 3205.

29 J. S. Ha, K. H. Kim and D. H. Choi, *J. Am. Chem. Soc.*, 2011, **133**, 10364; Y. N. Li, P. Sonar, S. P. Singh, M. S. Soh, M. van Meurs and J. Tan, *J. Am. Chem. Soc.*, 2011, **133**, 2198.

30 N. Sakai, J. Mareda, E. Vauthey and S. Matile, *Chem. Commun.*, 2010, **46**, 4225.

31 X. K. Gao, C. A. Di, Y. B. Hu, X. D. Yang, H. Y. Fan, F. Zhang, Y. Q. Liu, H. X. Li and D. Zhu, *J. Am. Chem. Soc.*, 2010, **132**, 3697; Y. Zhao, C. Di, X. Gao, Y. Hu, L. Zhang, Y. Liu, J. Wang, W. Hu and D. Zhu, *Adv. Mater.*, 2011, **23**, 2448; Y. Hu, X. Gao, C. Di, X. Yang, F. Zhang, Y. Liu, H. Li and D. Zhu, *Chem. Mater.*, 2011, **23**, 1204.

32 L. Tan, Y. Guo, G. Zhang, Y. Yang, D. Zhang, G. Yu, W. Xu and Y. Liu, *J. Mater. Chem.*, 2011, **21**, 18042.

33 L. E. Polander, S. P. Tiwari, L. Pandey, B. M. Seifried, Q. Zhang, S. Barlow, C. Risko, J. Brédas, B. Kippelen and S. R. Marder, *Chem. Mater.*, 2011, **23**, 3408.

34 S. Suraru, U. Zschieschang, H. Klauk and F. Würthner, *Chem. Commun.*, 2011, **47**, 11504.

35 *TTF Chemistry. Fundamentals and Applications of Tetrathiafulvalene*, ed. J. Yamada and T. Sugimoto, Springer Verlag, Heidelberg, 2004.

36 M. R. Bryce, *Adv. Mater.*, 1999, **11**, 11.

37 R. P. Shibaeva and E. B. Yagubskii, *Chem. Rev.*, 2004, **104**, 5347.

38 E. Coronado and P. Day, *Chem. Rev.*, 2004, **104**, 5419.

39 D. Canevet, M. Sallé, D. Q. Zhang, G. X. Zhang and D. Zhu, *Chem. Commun.*, 2009, 2245.

40 N. Martin, L. Sanchez, B. Illescas and I. Perez, *Chem. Rev.*, 1998, **98**, 2527; J. L. Segura and N. Martín, *Angew. Chem., Int. Ed.*, 2001, **40**, 1372.

41 E. Miyazaki, K. Takimiya and Y. Kunugi, *Chem. Mater.*, 2007, **19**, 5230; F. Otón, R. Pfattner, E. Pavlica, Y. Olivier, E. Moreno, J. Puigdollers, G. Bratina, J. Cornil, X. Fontrodona, M. Mas-Torrent, J. Veciana and C. Rovira, *Chem. Mater.*, 2011, **23**, 851; for single crystal TTF derivatives based OFETs: C. Rovira, *Chem. Rev.*, 2004, **104**, 5289.

42 K. Ueda, M. Goto, M. Iwamatsu, T. Sugimoto, S. Endo, N. Toyota, K. Yamamotob and H. Fujitac, *J. Mater. Chem.*, 1998, **8**, 2195.

43 X. Gao, W. Qiu, X. Yang, Y. Liu, Y. Wang, H. Zhang, T. Qi, Y. Liu, K. Lu, C. Du, Z. Shuai, G. Yu and D. Zhu, *Org. Lett.*, 2007, **9**, 3917.

44 C. Röger and F. Würthner, *J. Org. Chem.*, 2007, **72**, 8070.

45 Based on the low bond energy of the C–S bond, the decomposition of **1–6** may occur within TTF moieties above 230 °C. This is in agreement with the fact that the core-expanded NDI molecules with two 2-(1,3-dithiol-2-ylidene)malonitrile moieties start to decompose above 350 °C.[31] In addition, the absorption spectra of **1–6** in solution were almost unaltered after exposure to UV light as depicted in Fig. S34 and S35 (ESI†); thus, compounds **1–6** show good photochemical stability.

46 D. M. de Leeuw, M. M. J. Simenon, A. R. Brown and R. E. F. Einerhand, *Synth. Met.*, 1997, **87**, 53.

47 H. Usta, A. Facchetti and T. J. Marks, *J. Am. Chem. Soc.*, 2008, **130**, 8580.

48 Such intermolecular interactions among the electron donor and acceptor moieties may be due to the intermolecular arrangements in which the donor and acceptor moieties of neighboring molecules are closely arranged. Recent reports do indicate the existence of such intermolecular electron-donor and -acceptor arrangements (and electron-donor and acceptor interactions in the thin films of polymers with electron donor and acceptor moieties, see: H. N. Tsao, D. M. Cho, I. Park, M. R. Hansen, A. Mavrinskiy,

D. Y. Yoon, R. Graf, W. Pisula, H. W. Spiess and K. Müllen, *J. Am. Chem. Soc.*, 2011, **133**, 2605.
49 X. Zhan, A. Facchetti, S. Barlow, T. J. Marks, M. A. Ratner, M. R. Wasielewski and S. R. Marder, *Adv. Mater.*, 2011, **23**, 268.
50 E. J. Meijer, D. M. de Leeuw, S. Setayesh, E. van Veenendaal, B. H. Huisman, P. W. M. Blom, J. C. Hummelen, U. Scherf and T. M. Klapwijk, *Nat. Mater.*, 2003, **2**, 678.
51 D. J. Gundlach, J. E. Royer, S. K. Park, S. Subramanian, O. D. Jurchescu, B. H. Hamadani, A. J. Moad, R. J. Kline, L. C. Teague, O. Kirillov, C. A. Richter, J. G. Kushmerick, L. J. Richter, S. R. Parkin, T. N. Jackson and J. E. Anthony, *Nat. Mater.*, 2008, **7**, 216.
52 It is known that thin film morphology with larger grain size and better continuity is beneficial for high carrier mobility. In comparison, small grain size will result in many small interspaces which can capture charge carriers, leading to low carrier mobility, see: (*a*) H. Meng, Z. Bao, A. J. Lovinger, B. C. Wang and A. M. Mujsce, *J. Am. Chem. Soc.*, 2001, **123**, 9214; (*b*) Y. Wu, Y. Li, S. Gardner and B. S. Ong, *J. Am. Chem. Soc.*, 2005, **127**, 614.
53 The primary diffraction peaks appear at 3.7, 3.6 and 2.9° for thin films of **4–6**. Thus, the corresponding *d*-spacing are 23.5, 24.5 and 29 Å, respectively, which are close to that of the length (22 Å) of cores of **4–6** (with R = CH_3). These XRD data indicate that intermolecular side-alkyl chain (linked to TTF moieties) interdigitation may occur within thin films of **4–6**.
54 The primary diffraction peak for thin films of **1–3** appears at 4.3°, corresponding to a *d*-spacing of 20 Å. However, the width of **1–3** is estimated to be about 35 Å. Again, these XRD data reveal that intermolecular side-alkyl chain (at *N*,*N*′-positions of NDI moiety) interdigitation may occur within thin films of **1–3**.
55 K. B. Simonsen, N. Svenstrup, J. Lau, O. Simonsen, P. Mørk, G. J. Kristensen and J. Becher, *Synthesis*, 1996, 407; N. Narvor, N. Robertson, E. Wallace, J. D. Kilburn, A. E. Underhill, P. N. Bartlett and M. Webster, *J. Chem. Soc., Dalton Trans.*, 1996, 823; Y. Zhang, C. Wang, Y. Shen, L. Cai and G. Lai, *New J. Chem.*, 2008, **32**, 1968; J. Sly, P. Kasak, E. Gomar-Nadal, C. Rovira, L. Gorriz, P. Thordarson, D. B. Amabilino, A. E. Rowan and R. J. M. Nolte, *Chem. Commun.*, 2005, 1255.
56 W. R. Hatchard, *J. Org. Chem.*, 1964, **29**, 660.